Journal Pre-proof

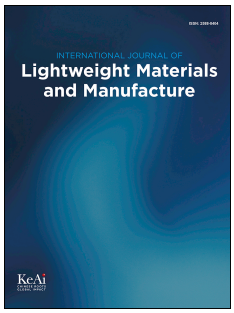

In-situ Reactive Synthesis and Characterization of a High Entropy Alloy Coating by Laser Metal Deposition

M. Dada, P. Popoola, N. Mathe, S. Pityana, S. Adeosun

PII: S2588-8404(21)00040-8

DOI: https://doi.org/10.1016/j.ijlmm.2021.09.002

Reference: IJLMM 172

To appear in: *International Journal of Lightweight Materials and Manufacture*

Received Date: 14 July 2021

Revised Date: 26 September 2021

Accepted Date: 27 September 2021

Please cite this article as: M Dada, P Popoola, N Mathe, S Pityana, S Adeosun, In-situ Reactive Synthesis and Characterization of a High Entropy Alloy Coating by Laser Metal Deposition, *International Journal of Lightweight Materials and Manufacture*, https://doi.org/10.1016/j.ijlmm.2021.09.002.

In-situ Reactive Synthesis and Characterization of a High Entropy Alloy Coating by Laser Metal Deposition

M Dada[1*], P Popoola[1], N Mathe[2], S Pityana[1, 2], S Adeosun[3]

[1] Department of Chemical, Metallurgical and Materials Engineering, Tshwane University of Technology, Staatsartillerie Rd, Pretoria West, Pretoria, 0183, South Africa
[2] National Laser Centre, Council for Scientific and Industrial Research, Meiring Naudé Road, Brummeria, Pretoria 0184, South Africa
[3] Department of Metallurgical and Materials Engineering, University of Lagos, University Road, Mainland Akoka, Yaba, Lagos, 100213, Nigeria
Corresponding author: dadadupeola@gmail.com

Abstract

In this study, we investigate the influence of *in situ* reactive synthesis of Ti6Al4V-AlCoCrFeNiCu high entropy alloys by laser metal deposition on the microstructural and mechanical properties of the as-built alloy as opposed to the traditional method of mixing powders via a ball mill prone to contamination and segregation. We explore the capability of a new alloy design by combining two base alloys via in situ reactive alloying, delivering the Ti6Al4V and AlCoCrFeNiCu high entropy alloy powders from multiple powder feeders and regulating their feed rate ratios. The nano mechanical, tribological and microstructural morphologies of the alloys were characterized using a nanoindentation tester, a tribometer, XRD and SEM, respectively. The results showed that satelliting the high entropy alloys powder and the Ti6Al4V powder fraction using double powder feedstock had a homogeneous distribution with dendritic structures. Optimization was achieved at a laser power of 1600 W, a scan speed of 12 mm/s and a powder flow rate of 2 g/min. The surface roughness (R_a) for Ti-6Al-4V, AlCoCrCuFeNi and (Ti-6Al-4V)-(AlCoCrCuFeNi) alloy was 0.5 μm, 0.63 μm and 0.80 μm, respectively. The high wear resistance of the novel Ti6Al4V- AlCoCrFeNiCu alloy was influenced by the hardness of the alloy which was higher than the Ti6Al4V alloy and the AlCoCrFeNiCu alloy. This study successfully defines the capabilities of *in situ* fabrication of high entropy alloys and presents novel techniques for multiple powder preparation of high entropy alloys using laser additive manufacturing, to permit the next generation of compositionally graded materials for aerospace components.

Keywords: Laser Deposition, in situ alloying, High Entropy Alloys, Tribology, Nanoindentation

1. Introduction

Ti-6Al-4V represents a class of functionally graded materials with excellent corrosion resistance, high strength to weight ratios and low density [1, 2]. These alloys with good mechanical and physical properties are widely used for aerospace applications [3]. Titanium-based alloys have a matrix comprising an alpha and beta phase that has aluminium and vanadium as an alpha and beta stabilizer, respectively [4]. However, the alloy's wear resistance is low and mechanical properties at elevated temperatures are poor limiting their application [5].

Over the past decade, High entropy alloys (HEAs) have become a research interest for scientists in the aerospace industry owing to their microstructural [6], electrochemical [7], magnetic [8], tribological [9], thermal [10] and mechanical properties [11]. The concept of HEAs is based on multiple principal elements with near equal or equal composition. Yeh et al. [12] reported that each principal element may contain a concentration of 35 and 5 atomic percentages. The authors first reported on the as-cast AlCoCrCuFeNi HEA, exhibiting FCC, B2 and BCC solid solution phases compared with traditional alloys which form intermetallic phases, making those traditional alloys brittle limiting their applications [13-15]. Thus, the AlCoCrCuFeNi HEA became one of the most studied HEA systems because it has some characteristic features such as good cold and hot workability, thermal stability, wear, fatigue, corrosion and oxidation resistance [16, 17]. However, the as-cast strength of the AlCoCrCuFeNi HEA is relatively low [18]. This can be attributed to the manufacturing process; therefore, the choice of the fabrication technique for improved properties is very important. Laser additive manufacturing (LAM) as a solid freeform technique fabricates HEAs into fully dense 3D shapes with a rapid solidification and cooling rate that improves the properties of the alloys compared with conventional technologies [19]. Most LAM processes have a layer thickness from 20 μm to 100 μm and a 70 cm^3/h build rate at 400 x 400 x 400 mm^3 build volume [19]. It allows mass personalization with low volume productions; it is also a net shape technique that saves cost and time by reducing production time and material waste [20]. Most metallic alloys fabricated via LAM in terms of the level of adoption and volume production are Ni-based superalloys, aluminium, steels, titanium alloys and more recently, high entropy alloys [20-24]. Ti-6Al-4V titanium-based alloy and high entropy alloys fabricated via LAM studied extensively comprises the high entropy alloy coating deposited on the Ti-6Al-4V alloy as a substrate to improve the properties of the titanium alloy. Zhang et al. [25] fabricated TiAlNiSiV HEA on a Ti-6Al-4V substrate, the results showed the HEA hardness was 4 to 6 times that of the substrate while the wear resistance was 5 to 4 times that of the Ti-6Al-4V alloy substrate, attributed to the solution and dispersion strengthening mechanism of the HEA. Chen et al. [26] coated AlTiVMoNb HEA on Ti-6Al-4V alloy to improve the oxidation resistance and surface hardness. The results showed that the hardness was 2.52 times that of the substrate and the oxidation resistance was 10.58% more than that of the Ti-6Al-4V substrate. To improve the tribological properties of the titanium alloy, Prabu et al. [27] fabricated AlCoCrCuFeNi HEA on a Ti-6Al-4V substrate. The results showed that the wear

resistance of the HEA was 2.62 times more than that of the Ti-6Al-4V substrate while the coefficient of friction of the HEA was 0.56 times higher than the Ti-6Al-4V substrate. Research on the enhancement of the tribological and mechanical properties of Ti-6Al-4V has led to the reinforcement of the alloy with hard particles like titanium nitride and zirconia but not with High entropy alloys [3, 28]. Laser-deposited high entropy alloys are a new class of materials with potential application as turbine engine components [29]. These materials used in the aerospace industry must be able to withstand extreme environmental high-temperature conditions. However, the mechanical properties of these alloys deteriorate over time, causing severe damages to crucial parts of the engine that may lead to malfunction during service, therefore, thorough investigation of these properties is important. Reports in the literature show that there can be as many as 7099 high entropy alloy systems, however, high entropy alloys have been extensively fabricated as coatings on Ti6Al4V substrates for aerospace turbine components and limited records show the design of (Ti6Al4V)–(AlCoCrFeNiCu) alloys using laser-deposition techniques. Furthermore, most reports in the literature on both alloys are based on the HEA fabricated on the Ti-6Al-4V substrate using pre alloyed powder for the feedstock deposition with limited work done on the combination of both alloys via in situ deposition producing the (Ti-6Al-4V)-(AlCoCrCuFeNi) HEA design system via LAM. [30]

The reduction of the anisotropy of Ti-based alloys during laser additive manufacturing under abrupt thermal gradients can be achieved via in-situ reactive synthesis [31]. Vora et al. [32] synthesized AlSi12 alloy using pre alloyed powders and in situ synthesis and the results showed that the in situ samples were more homogeneous and uniform than the pre alloyed samples. Wang et al. [33] examined the properties of a high entropy alloy using pre-alloyed powder via additive manufacturing. Although the authors recommend gas atomized powders as suitable for the fabrication of AM components, however, the study was limited to using only powder bed fusion via electron beam melting [34]. Martinez et al. [35] investigated the in situ alloying of Al-Cu12 using additive manufacturing. The result showed that the in situ Al-Cu12 samples had a maximum tensile strength compared to the as-cast pre alloyed Al-Cu12. Preheating was an effective method in obtaining chemical homogeneity and in situ synthesis was recommended as an innovative alloy design initiative that is cost-effective than the gas atomized pre alloyed powders. In situ alloying of powder, feedstocks provide flexibility and in-process modification of the as-built component with the possibilities of fabricating alloys with varying chemical

compositions. Cagirici et al. [36] did a comparative study of laser deposited HEAs via insitu alloying and thermophysical calculations. The authors proposed insitu alloying as a preferred technique for producing advanced novel alloys and the results showed that insitu alloying is a promising method for producing high entropy alloys without compromising their mechanical performance.

According to Xue et al. [37], Direct energy deposition fabricates complex and functionally graded components, therefore, this study attempts to develop novel compositionally graded materials by fabricating (Ti-6Al-4V)-(AlCoCrCuFeNi) HEAs via reactive in situ alloying using LAM to save material and energy cost.

2. Experimental Procedure

The Ti-based alloy powder with 45-90 microns was purchased from TLS, Germany while the HEA powder with 45-105 microns was purchased from F.J Brodmann & CO., L.L.C, USA. The as-received powders were deposited on a Ti6Al4V substrate with a dimension of 70 x 70 x 5 mm which was preheated at a temperature of 400°C after the substrate was grit blasted before the deposition to remove surface oxides. IPG fiber laser system located at the Council for Scientific and Industrial Research, Pretoria, South Africa (CSIR) was used in this study for deposition. The equipment with a coaxial feeding system and two powder hoppers with the nozzles supplying the powders are set to converge at the laser beam focal point during deposition. The Titanium-based alloy powder was loaded into a single powder feeder while the HEA powder was loaded in another. Therefore, only two separate powder feeders were used in this experiment to deliver the powders, thus, both powders were mixed *in situ* and fed into the melt pool through the nozzles. In this study, the rotational speed of the powder feeder was made constant at 2 (g/min), the groove was set at 4 mm (medium), the carrier gas at 2.0 l/min with a 50 % track overlap. The microstructural morphologies were investigated using JEOL-JSM-6010/LA plus Scanning Electron Microscope (SEM), Olympus BX_{51} light Optical Microscope and XPERT-PRO X-ray diffraction system (XRD). The cross-section of the samples was mounted, ground and polished to measure the surface roughness, nanomechanical and tribological properties using a Profilometer, an Anton-Paar TTX-NHT^3 Nanoindentation tester and TRB3 pin-on-disc tribometer, respectively, located at the Surface Engineering Research Laboratory (SERL), Pretoria South Africa.

Table 1 Laser Parameters for in situ (Ti-6Al-4V)-(AlCoCrCuFeNi) HEA

Alloy Composition	Laser Power (W)	Laser Scan Speed (mm/s)	Powder feed rate (g/min)	Energy Density J/mm^2	Gas flow rate (l/min)	Track Width (mm)	Track Depth (mm)	Track Height (mm)
(Ti-6Al-4V)-(AlCoCrCuFeNi)	1600.00	12	2.00	66.7	2.00	4	0.5	0.2

3. Results and Discussions

3.1 Powder Analysis

The as-received powders were analysed using a JEOL-JSM-6010/LA Plus Scanning electron microscope (SEM) equipped with an Energy Dispersive Spectrometer (EDS). The micrograph displayed in Figure 1 (a) and (b) shows the as-received Ti-based alloy and HEA alloy powders are somewhat spherical with a clean and smooth surface enough to flow freely from the nozzles during deposition. The chemical composition of the AlCoCrCuFeNi HEA powder and Ti-6Al-4V powder is shown in Tables 2 and 3 respectively.

The powders were gas atomized from the manufacturers, making the powders dense with improved quality. Susan et al. [44] reported that using high-quality powder with a spherical shape helps the LAM process melt the fine powders easily to produce net shape 3D components layer-by-layer. The authors concluded that intralayer porosity and lack of fusion found at the interlayer boundaries of powders are defects that can be prevented by optimizing the laser processing parameters. Limited work has been reported on the effects of the powder characteristics on the as-built LAM deposits, nonetheless, optimization of the laser parameters such as the powder feed rate, laser power and velocity significantly influences porosity and void formation during deposition [45]. Thus, the laser parameters used to synthesized the powders were derived from previous studies [46] and varied from 1200 W to 1600 W for the laser power, scan speed from 8 mm/s to 12 mm/s, at a flowrate of 2 g/min, however, optimization was obtained at 1600 W, 12 mm/s and a flowrate of 2 g/min, thus making these the optimal

parameters for the *in situ* deposition. Pores observed were probably caused when oxygen was released in a gaseous state during the highly exothermic reaction, resulting in partially or un-melted powder particles at lower laser power between 1200 W and 1400 W. The powder particles of the Ti-6Al-4V were allowed to stick to the AlCoCrCuFeNi HEA, resulting in a powder blend with the flow capacity suitable for producing good deposits. Nonetheless, some tracks are poorly bonded with the substrate which may be caused by a high powder flowrate, insufficient energy density or the inability of the feedstock to melt in the melt pool. It was observed that the particle ratios between the powder fractions with different chemical compositions or particle sizes can design multiple high entropy alloy compositional systems. Powder flowrate tests were conducted before deposition with the groove set at 4mm and argon carrier gas flowrate at 2 l/min. The Ti powder had a flowrate of 2.35 g/min while the High entropy alloy powder had a flowrate of 3.57 g/min. Consequently, deposition of Ti-6Al-4V-AlCoCrCuFeNi HEA can be achieved at a laser energy density of 66.7 J/mm^2 by in situ reaction synthesis with track width, depth and height at 4 mm, 0.5 mm and 0.4 mm respectively.

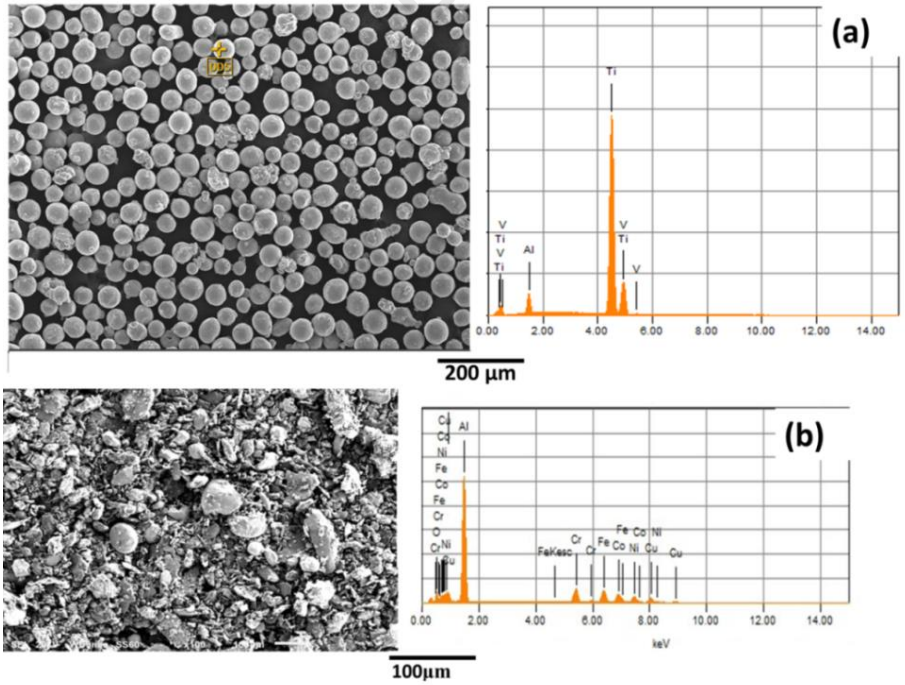

Fig.1. Micrographs of the powder morphology of (a) Ti-6Al-4V and; (b) AlCoCrCuFeNi HEA [47]

Table 2 Chemical composition of AlCoCrFeNiCu HEA in weight percentage

Element	Al (wt.%)	Co (wt.%)	Cr (wt.%)	Fe (wt.%)	Ni (wt.%)	Cu (wt.%)
AlCoCrFeNiCu	42.95	11.09	10.24	13.52	10.36	11.84

Table 3 Chemical composition of Ti6Al4V HEA in weight percentage

.

Element	Ti (wt.%)	Al (wt.%)	V (wt.%)
Ti6Al4V	87.89	6.71	5.4

3.2 Microstructural Analysis

According to Moore et al. [48], exothermic reactions play an important role in the *in situ* deposition of metals. Metal powders fed into the powder hoppers flows through the nozzles and into the laser focal zone to be melted in the molten pool before deposition. Once the powders are melted, the metal powders are in liquid form before fabrication. In the reaction between the Ti-6Al-4V alloy and AlCoCrCuFeNi HEA, the melting of the Ti-6Al-4V was significant as the dopant since the HEA have been previously fabricated using the set laser parameters[47]. The reaction velocity of Ti-6Al-4V, which is temperature-dependent, has been reported to be less than 10 cm/s in the liquid state [49]. The maximum particle size of the Ti-based alloy used in this study was 90 μm therefore; 0.9 x 10^{-3} s is estimated as the time taken for the full reaction to occur. Therefore, the Ti-6Al-4V - AlCoCrCuFeNi HEA can be fabricated once the base alloys in liquid states meet in the melt pool during deposition. From equation 6, the solidification velocity is equal to the travel speed multiplied by the angle between the melt pool, travel direction and the solidification front.

$$V_s = V_b x \cos\theta \ldots\ldots\ldots\ldots\ldots\ldots (1)$$

Where V is the solidification velocity,V_b is the travel speed and θ is the angle between the travel direction of the melt pool and the solidification front. The reaction velocity was higher than the solidification velocity and the travel speed of the molten pool to ensure the in situ alloying was homogenous. To decrease the thermal stresses of the laser deposition process, the substrate was

preheated to a temperature of 400 ℃ to produce defect-free deposits. The solidification rate and temperature gradient determined the structure of laser-deposited alloys. A dense columnar grain structure tilting towards the build direction was observed for the Ti-6Al-4V - AlCoCrCuFeNi HEA as seen in Figure 2. Ren et al. [30], also observed the columnar grains when studying the influence of volumetric energy density on the properties of near equiatomic AlCoCuFeNi HEA via laser deposition attributed to the epitaxial growth beside the temperature gradient.

The cross-sectional profile of the microstructure of the multiple tracks Ti-6Al-4V – AlCoCrCuFeNi deposition is shown in Figure 3. This clad consists of a hemispherical shape like deposit melted above the substrate surface with the thickness represented as C_T, the depth of the clad which shows the melt zone located below the surface of the substrate is represented as C_P , the dilution region showing the interface between the substrate and the clad is represented as C_D. The clad composition was homogeneously distributed with an inter-diffusion layer of approximately 7μm in thickness showing that the compositional change from the substrate to the alloy clad was quite steep. Porosity and inclusion were significantly reduced attributed to the successive deposition and remelting of the clad layer. Thermo-mechanical processing influences the morphology of an alloy structure. For the Ti-6Al-4V, the microstructures are characterized by the α and β phases which could either form bi-modal, equiaxed in this present study, needle-shaped lamellar structures [50]. These structures are formed depending on the rate of cooling from the β phase and the transus temperature. At higher cooling rates the grains are finer which during rapid quenching the martensitic transformation of the β phase occurs, thus leading to needle-shaped ultra-fine structures. These structures are characterized by improved hardness and moderate crystal lattice distortion [51]. On the other hand, the columnar dendritic structures were formed as a result of the solidification rates of the laser deposition. These structures most grow at a right angle and in a single direction, where the surface energy influences the growth rate [52]. These microstructures are also characterized by increased hardness and wear resistance [30] .

The XRD pattern in Figure 4, showed that the Ti-6Al-4V – AlCoCrCuFeNi had a predominant BCC phase made up of cubic structures comprising NiTi, TiCo and FeV and having diffraction peaks at, 42.614 °,64.478 °and 81.339 °with interplanar distances of 2.119 Å, 1.444 Å and 1.182 Å respectively. The dendritic structure of the alloy can be attributed to the rapid cooling rate of the laser-deposition process.

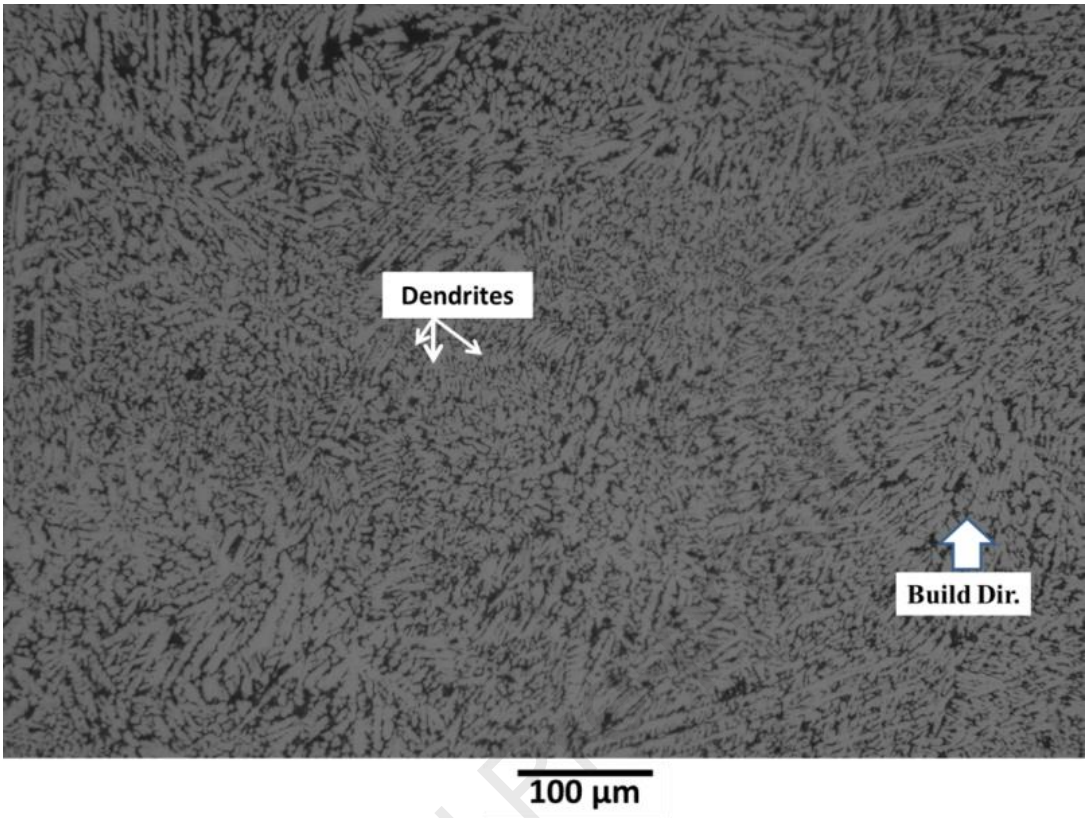

Fig.2. SEM Micrograph of the columnar dendritic structure of the in situ (Ti-6Al-4V)-(AlCoCrCuFeNi) alloy deposit

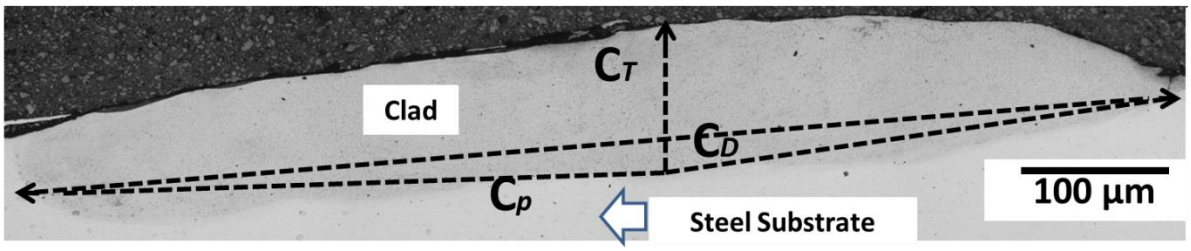

Fig.3. Microstructural Micrograph of in situ (Ti-6Al-4V)-(AlCoCrCuFeNi) alloy deposit

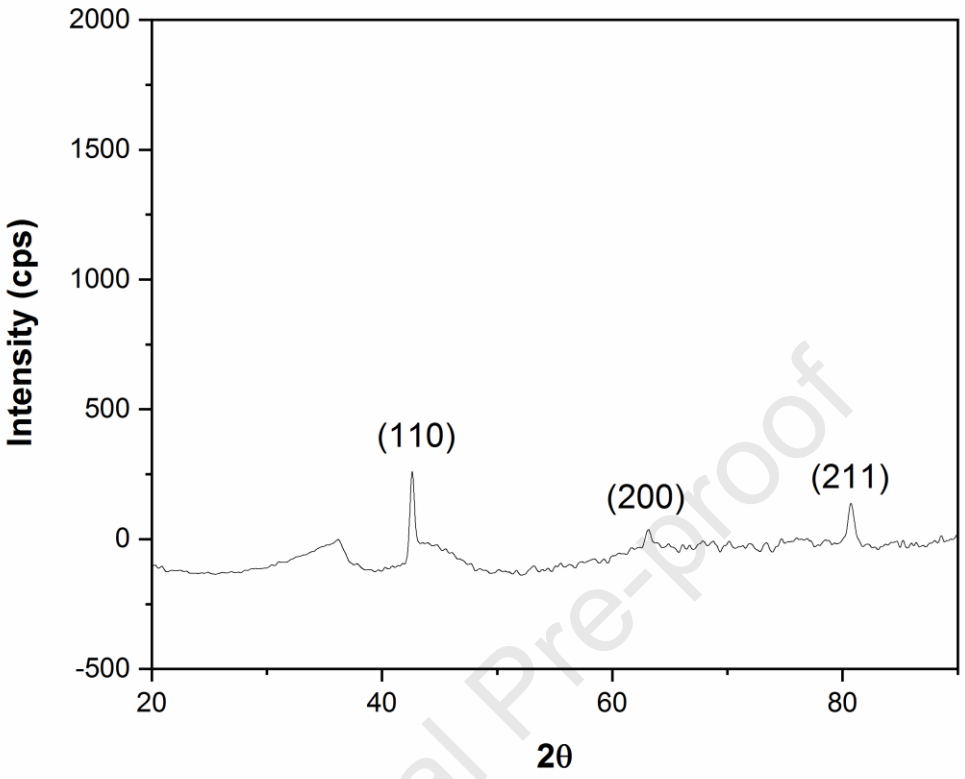

Fig.4. XRD patterns of *in situ* (Ti-6Al-4V)-(AlCoCrCuFeNi) HEAs deposit

3.3 Nanohardness Analysis

The mechanical property of the in situ (Ti-6Al-4V)-(AlCoCrCuFeNi) HEA was characterized using a force-controlled Anton Paar TTX-NHT^{3}Microindentation Tester. The instrument eliminates the effect of frame compliance on penetration depth measurement and thermal drift. The experiments were performed using the quick matrix mode with a maximum load of 200 mN, acquisition rate of 400.0 [Hz], the loading and unloading rates were at 600.00 mN/min. From Table 4, the mean modulus value of the (Ti-6Al-4V)-(AlCoCrCuFeNi) HEA were 2.867 GPa and 197.93 GPa, respectively, higher than the AlCoCrCuFeNi HEA and titanium alloys with modulus in the range of 105 GPa to 120 GPa [38, 53]. The nanoindentation tester was used to probe the mechanical behaviour of the BCC and FCC phases observed, with the load-displacement curves of different indentations shown in Figure 5 (a) and (b) while the impression of the indents is presented in Figure 6. The micrographs of the indents taken separately are shown in figure 6. The indentation on the BCC phase showed that the indentation depth

decreased as the indentation moved from 1 to 4 while relatively lower Vickers hardness was observed in the FCC phase ranging from 150 – 250 HV and the BCC phase had hardness as high as 724 HV attributed to the phase solid solution strengthening effect. Thus, the maximum penetration depth of the FCC phase at 1800 nm was greater than the BCC phase at 800 nm showing that the BCC phase is more resistant to plastic deformation than the FCC phase, also observed by Tung et al. [54]. Each indent has its indentation depths under the same load showing that the alloy has an extensive variant of particle mechanical properties [55]. Since the (Ti-6Al-4V)-(AlCoCrCuFeNi) HEA was predominantly BCC; the hardness of the alloy was approximately 67 % greater than the AlCoCrCuFeNi HEA and Ti-6Al-4V alloy, shown in Figure 7.

Table 4 Comparative study from literature

Alloy Composition	Fabrication Route	Modulus (GPa)	Hardness (GPa)	Ref
Ti-6Al-4V	Electron Beam Additive Manufacturing (EBAM)	127.9	6.5	[56]
AlCoCrCuFeNi	Laser Engineering Net Shaping (LENS)	149	2.77	[38]
(Ti-6Al-4V)-(AlCoCrCuFeNi)	Laser Engineering Net Shaping (LENS)	197	2.8	This Study

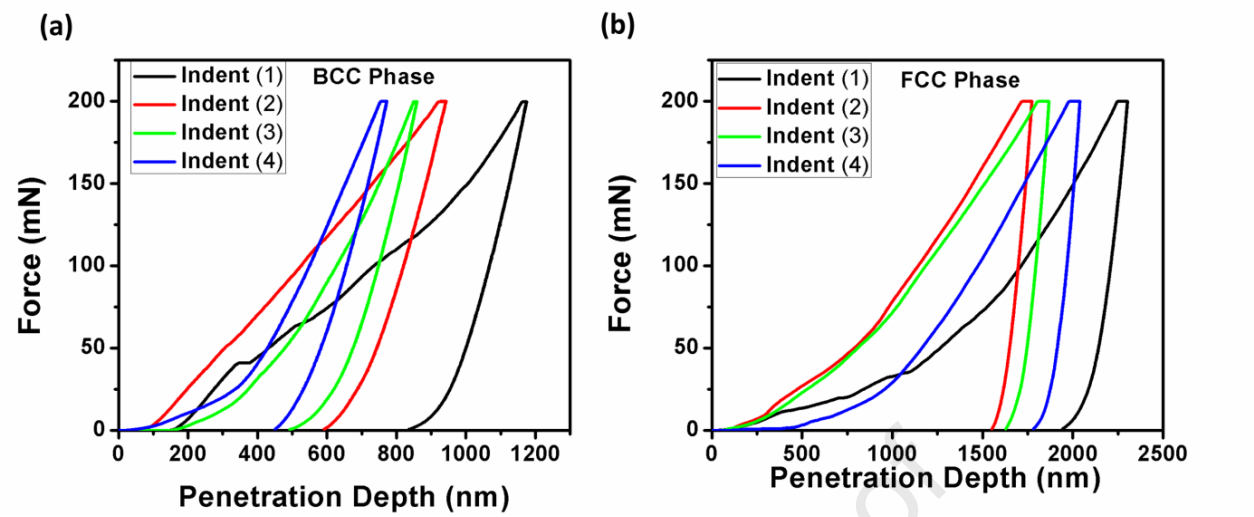

Fig.5. Comparison of indentation compression curves for the (Ti-6Al-4V)-(AlCoCrCuFeNi) HEA deposit

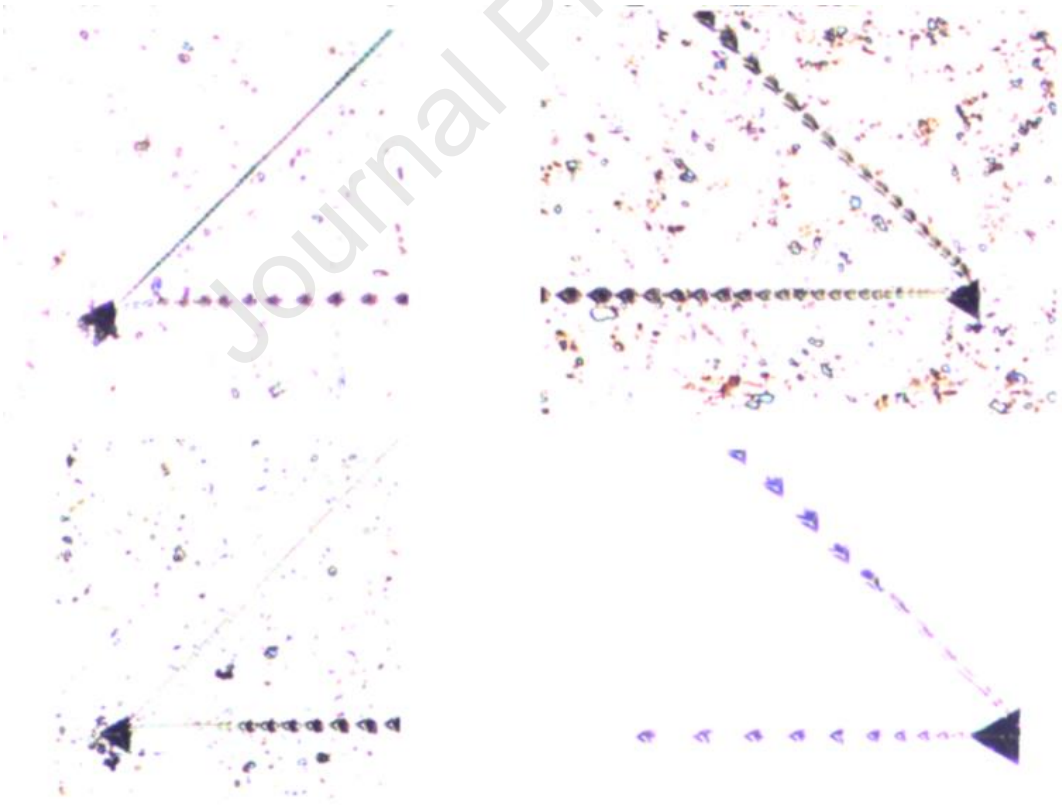

Fig.6. Impression of the Indents captured separately at a load of 200 mN

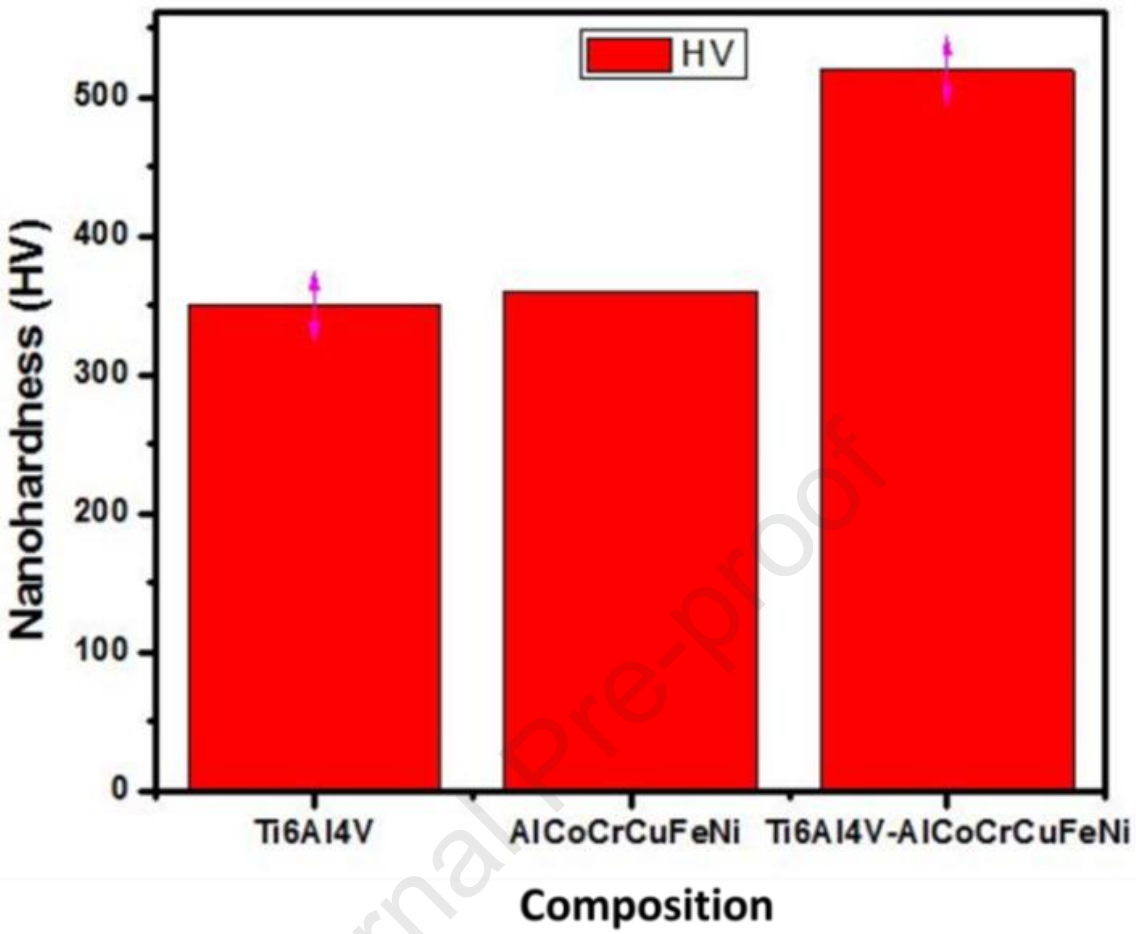

Fig.7. Microhardness profile of Ti-6Al-4V, AlCoCrCuFeNi and (Ti-6Al-4V)-(AlCoCrCuFeNi) Alloy

Based on the Oliver & Pharr method, the modulus and nanohardness of the different phases in the (Ti-6Al-4V)-(AlCoCrCuFeNi) HEA were extracted from the load-displacement curves. As shown in Figure 8, the hardness of the BCC phase increased by 184 % from 7.820 to 22.212 GPa and the modulus increased by~ 70 % from 192 to 328 GPA. In contrast, the hardness and modulus of the FCC phase decreased by~38 % from 2.997 to 2.178 GPa and 17 % from 172 to 147 GPa, respectively, as the indent moved from 1 to 4. This verifies that the solid strengthening mechanism of the phases differs and that the solid strengthening mechanism is more distinct in the BCC phase.

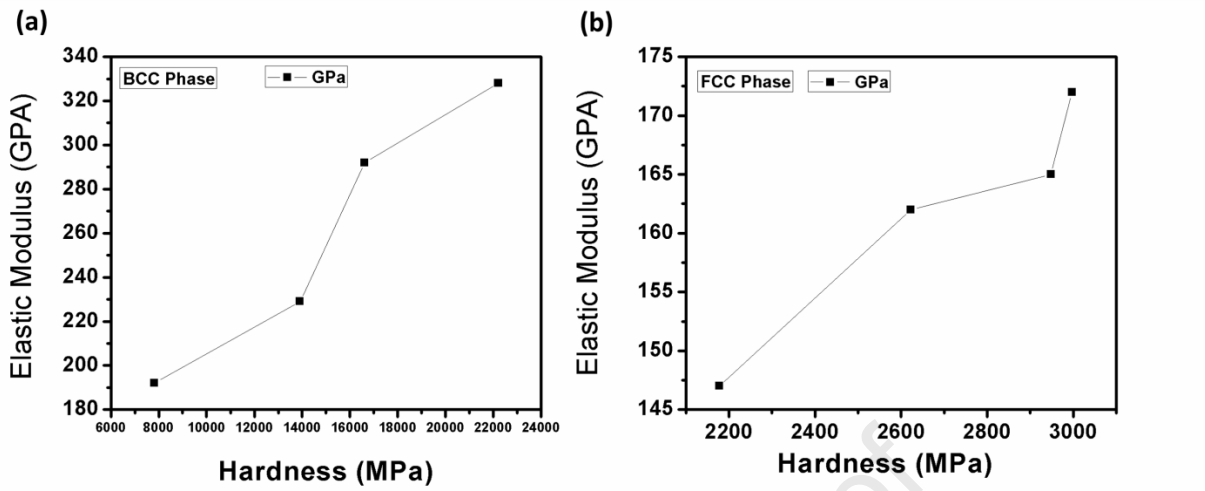

Fig.8. NanoHardness and Young Moduli of the phases observed in the (Ti-6Al-4V)-(AlCoCrCuFeNi) HEA

3.4 Wear Analysis

The examination of the tribological behaviour of the Ti-6Al-4V, AlCoCrCuFeNi and (Ti-6Al-4V)-(AlCoCrCuFeNi) alloy under sliding wear conditions were achieved via a ball-on-disk test on a TRB3 pin-on-disc tribometer with the samples clamped down for rotational motion and a spherical ball made up of steel with 1 mm diameter serving as the counter material with a 10, 15 and 20 N force at room temperature. There were at least three repetitions of the tests. The surface roughness, wear rate and coefficient of friction were derived through profilometer and Instrumx 8.1.8 software. The results showed that the mean surface roughness (R_a) for Ti-6Al-4V, AlCoCrCuFeNi and (Ti-6Al-4V)-(AlCoCrCuFeNi) alloy were 0.5 μm, 0.63 μm and 0.80 μm, respectively. The (Ti-6Al-4V)-(AlCoCrCuFeNi) alloy is predominantly BCC dendritic attributed to the high Al content which is characteristic of spinodal decomposition with modulated structures. The spinodal decomposition of the predominant BCC phase provides the alloy with a nano-composite strengthening effect which invariably improves the wear resistance of the alloy by resisting plastic deformation. Consequently, Figure 9 shows that the (Ti-6Al-4V)-(AlCoCrCuFeNi) had the highest wear resistance with the lowest wear rate of 1.096 x 10^{-6} mm^3/mN compared with AlCoCrCuFeNi and Ti-6Al-4V alloys which had wear rates values of 4.267 x 10^{-6} mm^3/mN and 6.511 x 10^{-6} mm^3/mN, respectively, attributed to the hardness properties. This is in agreement with the conclusion provided by Khruschov, which states that

the hardness of a material is generally proportional to its wear resistance [43]. It was observed that there was very little influence of the applied force from 10 N to 15 N on the sliding wear behaviour of the alloys at ambient temperature until the force was increased to 20 N. For the (Ti-6Al-4V)-(AlCoCrCuFeNi), AlCoCrCuFeNi and Ti-6Al-4V alloy, the average coefficient of friction (COF) measured was 0.4, 0.5 and 0.6, respectively, as shown in Figure 10. The wear track of the (Ti-6Al-4V)-(AlCoCrCuFeNi) HEA was examined using SEM and Optical Microscope. Figure 11 shows the high entropy alloy experienced abrasive wear with particles and hard oxidized debris observed on the worn surface also observed by Zhang et al. [57].

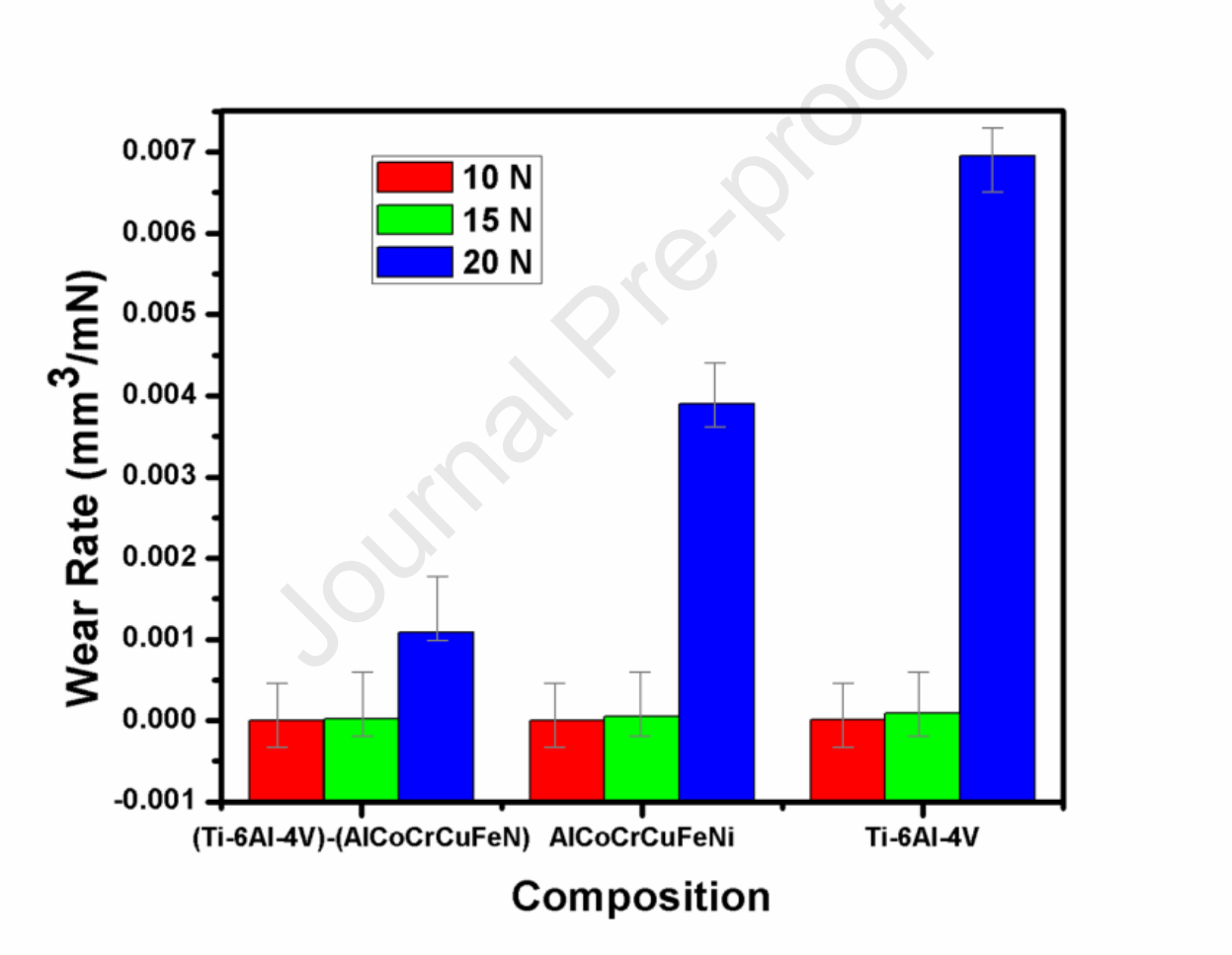

Fig.9. Wear rates of (Ti-6Al-4V)-(AlCoCrCuFeNi), AlCoCrCuFeNi and Ti-6Al-4V

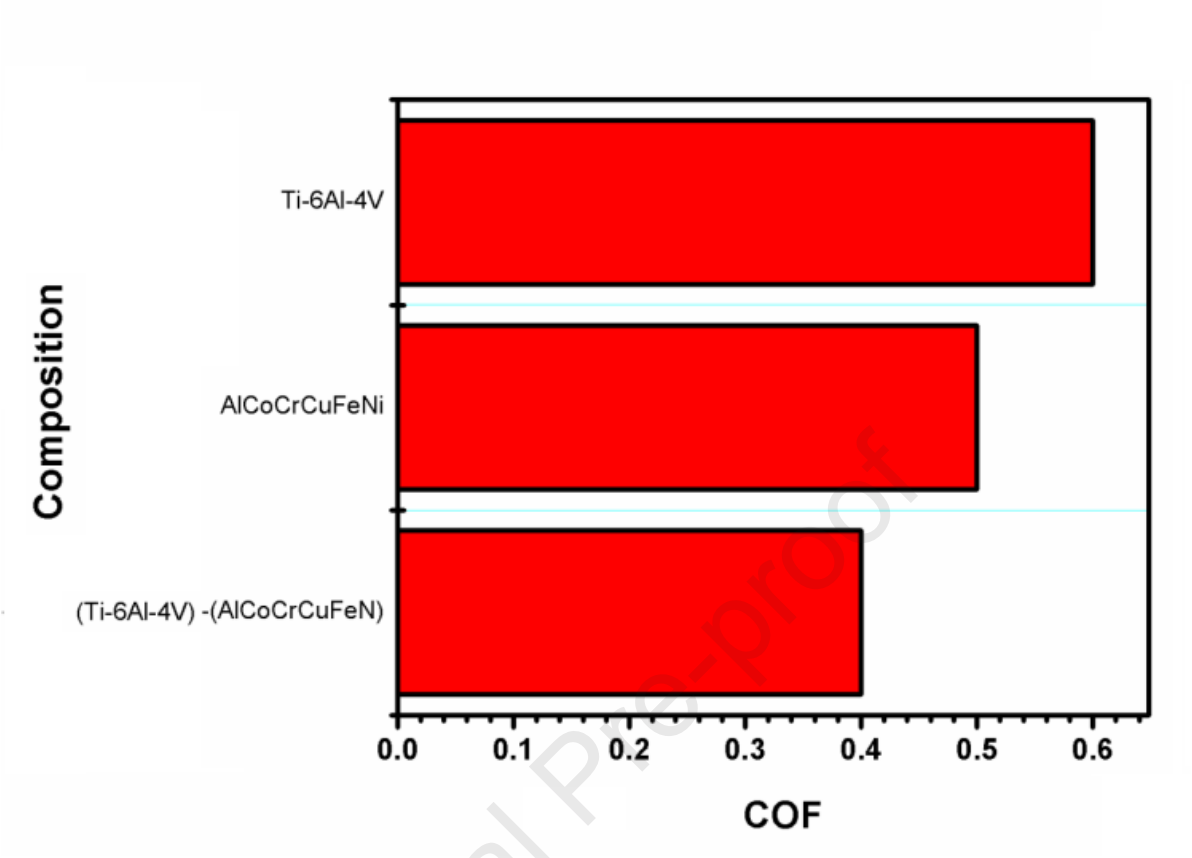

Fig.10. Average Coefficient of friction for (Ti-6Al-4V)-(AlCoCrCuFeNi), AlCoCrCuFeNi and Ti-6Al-4V alloys at room temperature

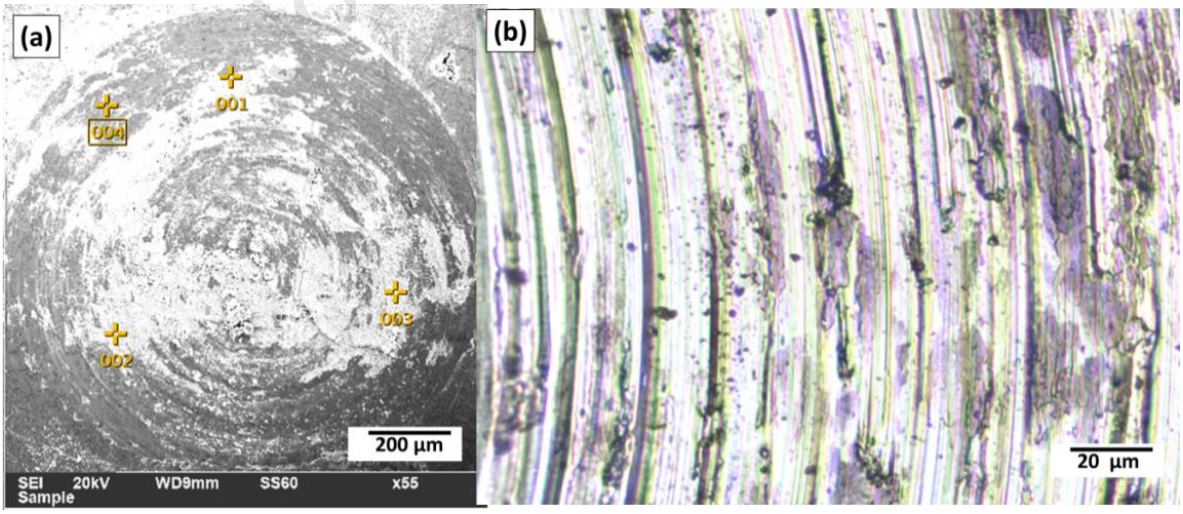

Fig.11. (a) SEM of the Wear Track for (Ti-6Al-4V)-(AlCoCrCuFeNi) (b) Optical micrographs of the worn scar for (Ti-6Al-4V)-(AlCoCrCuFeNi)

4. Conclusions

This study investigates innovative ways of fabricating equal or near- equal high entropy alloy systems via reactive in situ alloying using laser additive manufacturing. The (Ti-6Al-4V)-(AlCoCrCuFeNi) HEA was fabricated using laser parameters; laser power 1600 W, scan speed 12 mm/s and flow rate of 2 g/min from two powder feeders. The influence of the *in situ* reactive synthesis of Ti6Al4V- AlCoCrFeNiCu high entropy alloys on the microstructural and mechanical properties of the as-built alloy were studied.

- Quality track deposits with homogeneous columnar dendritic structures comprising predominantly BCC phase were observed attributed to the rapid solidification and cooling rates of the laser-deposition process and the exothermic reaction between the Ti-6Al-4V and AlCoCrCuFeNi alloy.
- The hardness and modulus of the BCC phase increased by 184 % and 70 % while the hardness and modulus of the FCC phase decreased by ~ 38 % and by 17 %, respectively, showing that the solid strengthening mechanism of the phases differs and that the solid strengthening mechanism is more distinct in the BCC phase.
- The (Ti-6Al-4V)-(AlCoCrCuFeNi) alloy fabricated via in situ synthesis showed improved mechanical properties compared with the AlCoCrCuFeNi and Ti-6Al-4V alloys, showing the capabilities of the in-situ processing in producing alloys with improved properties.
- The *in-situ* fabricated (Ti-6Al-4V)-(AlCoCrCuFeNi) HEA presents alternative techniques in producing innovative high entropy alloy compositions via laser additive manufacturing as opposed to the use of conventional pre alloyed feedstock powders. Thus, the elimination of the prealloying powder process saves time and reduces the lifecycle costs of production.

Acknowledgement

The authors will like to appreciate Mr Samuel Skhosane at the Council for Scientific and Industrial Research (CSIR), the National Laser Center (Laser Enabled Manufacturing Resource Group), Mr Juwon Ojo Fayomi and Uyor Uwa Orji at the Surface Engineering Research Laboratory (SERL), Tshwane University of Technology, Pretoria, South Africa for their technical support during this research.

References

1. Kumar, M.S., et al., *Characterisation of titanium–titanium boride composites processed by powder metallurgy techniques.* Materials characterization, 2012. **73**: p. 43-51.
2. Kondoh, K., et al., *High-temperature properties of extruded titanium composites fabricated from carbon nanotubes coated titanium powder by spark plasma sintering and hot extrusion.* Composites science and technology, 2012. **72**(11): p. 1291-1297.
3. Kabir, A.S.H., et al., *Effect of postweld heat treatment on microstructure, hardness, and tensile properties of laser-welded Ti-6Al-4V.* Metallurgical and Materials Transactions A, 2012. **43**(11): p. 4171-4184.
4. Pederson, R., *Microstructure and phase transformation of Ti-6Al-4V*. 2002, Luleå tekniska universitet.
5. Obadele, B.A., et al., *Effect of ZrO2 addition on the dry sliding wear behavior of laser clad Ti6Al4V alloy.* Wear, 2015. **328**: p. 295-300.
6. Zhang, Y., et al., *Microstructures and properties of high-entropy alloys.* Progress in Materials Science, 2014. **61**: p. 1-93.
7. Chen, Y., et al., *Microstructure and electrochemical properties of high entropy alloys—a comparison with type-304 stainless steel.* Corrosion science, 2005. **47**(9): p. 2257-2279.
8. Lucas, M., et al., *Magnetic and vibrational properties of high-entropy alloys.* Journal of Applied Physics, 2011. **109**(7): p. 07E307.
9. Lin, D.-y., et al., *Tribological properties of FeCoCrNiAlB x high-entropy alloys coating prepared by laser cladding.* Journal of Iron and Steel Research International, 2017. **24**(2): p. 184-189.
10. Ge, H., F. Tian, and Y. Wang, *Elastic and thermal properties of refractory high-entropy alloys from first-principles calculations.* Computational Materials Science, 2017. **128**: p. 185-190.
11. Li, Z., et al., *Mechanical properties of high-entropy alloys with emphasis on face-centered cubic alloys.* Progress in Materials Science, 2019. **102**: p. 296-345.
12. Yeh, J.W., et al., *Nanostructured high-entropy alloys with multiple principal elements: novel alloy design concepts and outcomes.* Advanced Engineering Materials, 2004. **6**(5): p. 299-303.
13. Lindsay, G., *Confusion by design.* Nature, 1993. **366**(25): p. 303-304.
14. Burke, E., B. Chalmers, and J. Krumhansl, *Thermodynamics of Solids*. 1991, John Wiley & Sons, New York.
15. Gwalani, B., et al., *High-entropy alloy strengthened by in situ formation of entropy-stabilized nano-dispersoids.* Scientific reports, 2018. **8**(1): p. 1-9.
16. Jien-Wei, Y., *Recent progress in high entropy alloys.* Ann. Chim. Sci. Mat, 2006. **31**(6): p. 633-648.
17. Hemphill, M.A., et al., *Fatigue behavior of Al0. 5CoCrCuFeNi high entropy alloys.* Acta Materialia, 2012. **60**(16): p. 5723-5734.
18. Chen, H., et al. *Effect of the substitution of Co by Mn in Al-Cr-Cu-Fe-Co-Ni high entropy alloys*. in *Annales De Chimie-Science Des Materiaux*. 2006. Paris; New York: Masson, 1978-.
19. Gorsse, S., et al., *Additive manufacturing of metals: a brief review of the characteristic microstructures and properties of steels, Ti-6Al-4V and high-entropy alloys.* Science and Technology of advanced MaTerialS, 2017. **18**(1): p. 584-610.
20. Sames, W.J., et al., *The metallurgy and processing science of metal additive manufacturing.* International materials reviews, 2016. **61**(5): p. 315-360.
21. Sallamand, P. and J. Pelletier, *Laser cladding on aluminium-base alloys: microstructural features.* Materials Science and Engineering: A, 1993. **171**(1-2): p. 263-270.

22. Xu, P., et al., *Wear and corrosion resistance of laser cladding AISI 304 stainless steel/Al2O3 composite coatings.* Surface and Coatings Technology, 2014. **238**: p. 9-14.
23. Weng, F., C. Chen, and H. Yu, *Research status of laser cladding on titanium and its alloys: A review.* Materials & Design, 2014. **58**: p. 412-425.
24. Qiu, X.-W. and C.-G. Liu, *Microstructure and properties of Al2CrFeCoCuTiNix high-entropy alloys prepared by laser cladding.* Journal of Alloys and Compounds, 2013. **553**: p. 216-220.
25. Zhang, H., et al., *Microstructure and wear resistance of TiAlNiSiV high-entropy laser cladding coating on Ti-6Al-4V.* Journal of Materials Processing Technology, 2020. **282**: p. 116671.
26. Chen, L., et al., *Lightweight refractory high entropy alloy coating by laser cladding on Ti–6Al–4V surface.* Vacuum, 2021. **183**: p. 109823.
27. Prabu, G., et al., *Microstructural Evolution and Wear Behavior of AlCoCrCuFeNi High Entropy Alloy on Ti–6Al–4V Through Laser Surface Alloying.* Metals and Materials International, 2020: p. 1-13.
28. Obadele, B.A., et al., *Improving the tribocorrosion resistance of Ti6Al4V surface by laser surface cladding with TiNiZrO2 composite coating.* Applied Surface Science, 2015. **345**: p. 99-108.
29. Zhao, D., et al., *Ordered nitrogen complexes overcoming strength–ductility trade-off in an additively manufactured high-entropy alloy.* Virtual and Physical Prototyping, 2020. **15**(sup1): p. 532-542.
30. Ren, Y., et al., *Effect of volumetric energy density on microstructure and tribological properties of FeCoNiCuAl high-entropy alloy produced by laser powder bed fusion.* Virtual and Physical Prototyping, 2020. **15**(sup1): p. 543-554.
31. Mosallanejad, M.H., et al., *In-situ alloying in laser-based additive manufacturing processes: A critical review.* Journal of Alloys and Compounds, 2021: p. 159567.
32. Vora, P., et al., *AlSi12 in-situ alloy formation and residual stress reduction using anchorless selective laser melting.* Additive manufacturing, 2015. **7**: p. 12-19.
33. Wang, P., et al., *Additively manufactured CoCrFeNiMn high-entropy alloy via pre-alloyed powder.* Materials & Design, 2019. **168**: p. 107576.
34. Montero-Sistiaga, M.L., et al., *Changing the alloy composition of Al7075 for better processability by selective laser melting.* Journal of Materials Processing Technology, 2016. **238**: p. 437-445.
35. Martinez, R., I. Todd, and K. Mumtaz, *In situ alloying of elemental Al-Cu12 feedstock using selective laser melting.* Virtual and Physical Prototyping, 2019. **14**(3): p. 242-252.
36. Cagirici, M., et al., *Additive manufacturing of high-entropy alloys by thermophysical calculations and in situ alloying.* Journal of Materials Science & Technology, 2021. **94**: p. 53-66.
37. Xue, P., et al., *Effect of laser incident energy on the densification and structure–property relationships of additively manufactured CrCoNi medium-entropy alloy.* Virtual and Physical Prototyping, 2021: p. 1-13.
38. Dada, M., et al., *Investigating the elastic modulus and hardness properties of a high entropy alloy coating using nanoindentation.* International Journal of Lightweight Materials and Manufacture, 2021. **4**(3): p. 339-345.
39. Masanta, M., S. Shariff, and A.R. Choudhury, *Evaluation of modulus of elasticity, nano-hardness and fracture toughness of TiB2–TiC–Al2O3 composite coating developed by SHS and laser cladding.* Materials Science and Engineering: A, 2011. **528**(16-17): p. 5327-5335.

40. Franco Jr, A.R., et al., *The use of a Vickers indenter in depth sensing indentation for measuring elastic modulus and Vickers hardness.* Materials Research, 2004. **7**(3): p. 483-491.
41. Wu, Z., et al., *Microstructure characterization of AlxCo1Cr1Cu1Fe1Ni1 (x= 0 and 2.5) high-entropy alloy films.* Journal of alloys and compounds, 2014. **609**: p. 137-142.
42. Hynowska, A., et al., *Nanostructured β-phase Ti–31.0 Fe–9.0 Sn and sub-μm structured Ti–39.3 Nb–13.3 Zr–10.7 Ta alloys for biomedical applications: Microstructure benefits on the mechanical and corrosion performances.* Materials Science and Engineering: C, 2012. **32**(8): p. 2418-2425.
43. Ayatollahi, M. and A. Karimzadeh, *Nano-indentation measurement of fracture toughness of dental enamel.* International Journal of Fracture, 2013. **183**(1): p. 113-118.
44. Susan, D., et al., *Quantitative characterization of porosity in stainless steel LENS powders and deposits.* Materials Characterization, 2006. **57**(1): p. 36-43.
45. Rabin, B., G. Smolik, and G. Korth, *Characterization of entrapped gases in rapidly solidified powders.* Materials Science and Engineering: A, 1990. **124**(1): p. 1-7.
46. Dada, M., et al., *Process optimization of high entropy alloys by laser additive manufacturing.* Engineering Reports, 2020. **2**(10): p. e12252.
47. Dada, M., et al., *Process optimization of high entropy alloys by laser additive manufacturing.* Engineering Reports, 2020: p. e12252.
48. Moore, J.J. and H. Feng, *Combustion synthesis of advanced materials: Part I. Reaction parameters.* Progress in materials science, 1995. **39**(4-5): p. 243-273.
49. Duckham, A., et al., *Reactive nanostructured foil used as a heat source for joining titanium.* Journal of applied physics, 2004. **96**(4): p. 2336-2342.
50. Sieniawski, J., et al., *Microstructure and mechanical properties of high strength two-phase titanium alloys.* Titanium alloys-advances in properties control, 2013: p. 69-80.
51. Joshi, V.A., *Titanium alloys: an atlas of structures and fracture features*. 2006: Crc Press.
52. Zaeem, M.A., H. Yin, and S.D. Felicelli, *Modeling dendritic solidification of Al–3% Cu using cellular automaton and phase-field methods.* Applied Mathematical Modelling, 2013. **37**(5): p. 3495-3503.
53. Abdulrahman, K.O., et al., *Effect of laser power on the microstructure and mechanical properties of laser deposited titanium aluminide composite.* Advances in Materials and Processing Technologies, 2021: p. 1-12.
54. Tung, C.-C., et al., *On the elemental effect of AlCoCrCuFeNi high-entropy alloy system.* Materials letters, 2007. **61**(1): p. 1-5.
55. Gu, S., et al., *Characterization of local mechanical properties of laser-cladding H13–TiC composite coatings using nanoindentation and finite element analysis.* Materials & Design, 2012. **39**: p. 72-80.
56. Gong, X., et al. *Microstructural analysis and nanoindentation characterization of TI-6AL-4V parts from electron beam additive manufacturing*. in *ASME International Mechanical Engineering Congress and Exposition*. 2014. American Society of Mechanical Engineers.
57. Zhang, Y., et al., *Effect of process parameters on the microstructure and properties of laser-clad FeNiCoCrTi0. 5 high-entropy alloy coating.* Int. J. Miner. Metall. Mater., 2020. **27**(5): p. 630.

Conflict of Interest: Authors declare that there are no conflicts of interest